Applied Catalysis B: Environmental 342 (2024) 123339

Contents lists available at ScienceDirect

Applied Catalysis B: Environmental

journal homepage: www.elsevier.com/locate/apcatb

# Amide-assisted synthesis of TS-1 zeolites with active $Ti(OH_2)_2(OH)_2(OSi)_2$ sites toward efficient oxidative desulfurization

Jiani Zhang [a], Risheng Bai [a], Zhaochi Feng [b], Jiyang Li [a,*]

[a] State Key Laboratory of Inorganic Synthesis and Preparative Chemistry, College of Chemistry, Jilin University, Changchun 130012, China
[b] State Key Laboratory of Catalysis, Dalian Institute of Chemical Physics, Chinese Academy of Sciences, 457 Zhongshan Road, Dalian 116023, China

ARTICLE INFO

*Keywords:*
TS-1 zeolite
Active-site microenvironment
Hexa-coordinated Ti site
Amide-assisted method
Oxidative desulfurization

ABSTRACT

Aiming to promote the activity of TS-1 zeolite in catalytic oxidative desulfurization (ODS), a general amide-assisted strategy was proposed to synthesize hierarchical TS-1 zeolite with rich and homogeneously distributed $Ti(OH_2)_2(OH)_2(OSi)_2$ species. Strong interactions between acrylamide (AM) and Si/Ti as well as self-polymerization of AM in synthetic gels change the zeolite formation process, thus to effectively construct Ti $(OH_2)_2(OH)_2(OSi)_2$, promote Ti evenly distribution and form micro-mesopore structure. The activity of Ti $(OH_2)_2(OH)_2(OSi)_2$ was evaluated by ODS of refractory sulfur-containing compounds. The advantages of Ti $(OH_2)_2(OH)_2(OSi)_2$ over $TiO_4$ in substrate adsorption and reactive intermediate formation for ODS were further proved by theoretical calculations. By adjusting AM amount to optimize the $Ti(OH_2)_2(OH)_2(OSi)_2$ content and distribution, the obtained catalyst achieves 134.8 $h^{-1}$ of turnover frequency and 100 % DBT removal at ten minutes, and maintains > 92 % removal after seven cycles at 333 K. This facile active-site construction strategy is promising to be extended to other heteroatom-containing zeolite catalysts.

## 1. Introduction

Despite the recent emergence and promotion of new energy strategies, traditional fuels continue to dominate as the primary energy source. The growing and disturbing environmental issues arising from the combustion of sulfur-containing diesel fuel have forced the adoption of more stringent emission standards for sulfur content [1,2]. Hydrodesulfurization (HDS) is a conventional desulfurization technology used in industry, which requires high temperature and high hydrogen pressure, and is difficult to remove heavier oil fractions [3,4]. Conversely, oxidative desulfurization (ODS) has emerged as a highly promising alternative technology because of its mild and easily available reaction conditions and ultra-deep removal of refractory aromatic sulfur compounds. The development of high-performance catalysts including Ti-containing porous materials is the crucial issue of ODS technology [5–9].

Titanosilicate zeolites such as TS-1 (**MFI**), Ti-MOR (**MOR**), Ti-MWW (**MWW**), and Ti-Beta (***BEA**) can act as redox catalysts due to the incorporation of titanium atoms into the framework, thus providing new choices for various oxidation reactions including ODS [6,10–16]. Compared with other titanium-containing zeolites, TS-1 zeolites offer distinct advantages of facile synthesis, exceptional thermal stability and remarkable adaptability in tailoring the pore structures, which are more conducive to the application and industrialization in ODS [17–23]. However, TS-1 zeolites, characterized by their microporous structure, present a challenge in facilitating interactions among the bulky substrate, organic hydrogen peroxide, and the active Ti sites [18,20,24,25]. Furthermore, the lattice Ti content of TS-1 zeolites is limited because of the spatial site resistance, typically less than 2 wt% (Si/Ti = 40), thus the catalytic performance of TS-1 can hardly be further enhanced by increasing the $TiO_4$ content [26–28]. Therefore, there exists a pressing need to enhance the inherent activity and accessibility of restricted Ti sites by modulating their coordination, microenvironment and uniform distribution.

To date, Ti active centres with different coordination environments have been identified in TS-1 zeolite. Apart from tetra-coordinated $TiO_4$ as the main active sites, the tetra-coordinated dinuclear Ti, tetra-coordinated $Ti(OSi)_3OH$, penta-coordinated $Ti(OH)_2(OSi)_3$, hexa-coordinated $Ti(OH_2)_2(OH)_2(OSi)_2$ and $Ti(OH)_4(OSi)_2$ have been found and proven to possess enhanced activity than traditional $TiO_4$ in olefin epoxidation [28–32]. As for the ODS, although limited investigations have indicated that $Ti(OH_2)_2(OH)_2(OSi)_2$ species outperform $TiO_4$

* Corresponding author.
*E-mail address:* lijiyang@jlu.edu.cn (J. Li).

https://doi.org/10.1016/j.apcatb.2023.123339
Received 25 July 2023; Received in revised form 15 September 2023; Accepted 25 September 2023
Available online 26 September 2023

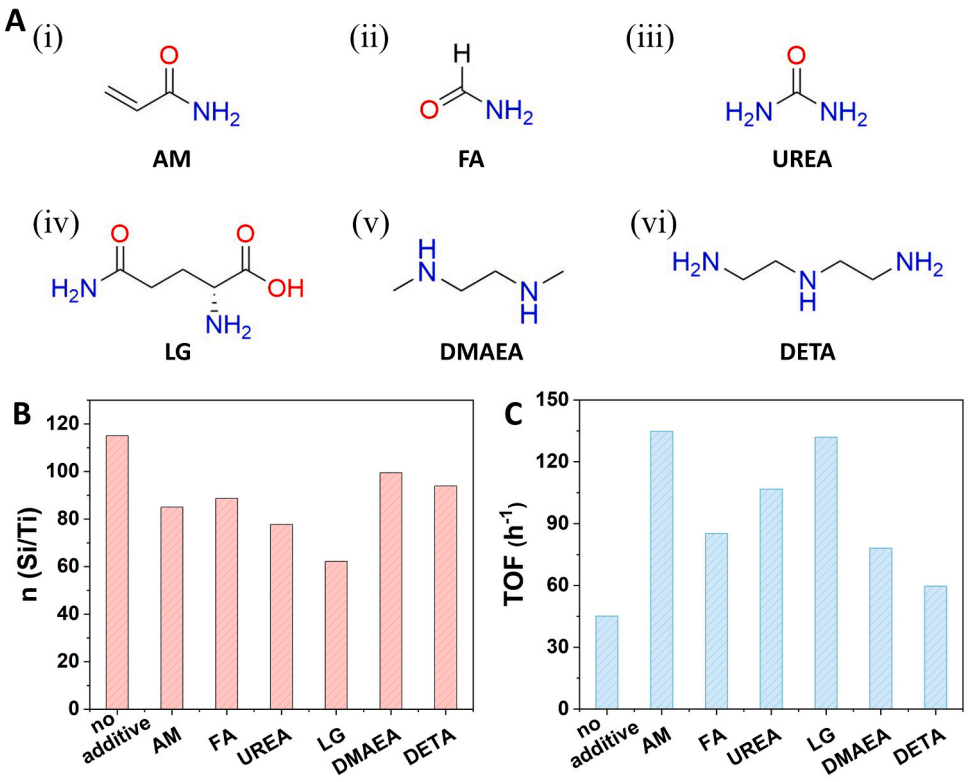


**Fig. 1.** (A) Additive structures for syntheses of TS-1 zeolites, in which (i) acrylamide (AM), (ii) formamid (FA), (iii) urea (UREA), (iv) L-glutamine (LG), (v) N,N′-dimethylethylenediamine (DMAEA) and (vi) diethylenetriamine (DETA). (B) Si/Ti molar ratio determined by ICP and (C) TOF for DBT oxidation of samples synthesized with different additives.

species [33], a fundamental and in-depth understanding of the precise mechanisms underlying their superior activity remains elusive. Moreover, the construction methods of active $Ti(OH_2)_2(OH)_2(OSi)_2$ in TS-1, such as post-treatment, the addition of amino acids or polymeric polyacrylamide, and seed-assisted microwave irradiation suffer from poor controllability and complex synthesis procedures [28,32,34–36]. The rich $Ti(OH_2)_2(OH)_2(OSi)_2$ and their uniform distribution are difficult to be achieved via these methods.

Herein, a facile and effective amide-assisted strategy has been developed to successfully construct homogeneous distributed Ti $(OH_2)_2(OH)_2(OSi)_2$ sites and mesoporous structure in TS-1 zeolite. The systematic characterizations have been performed to reveal the effect of amide additive in the crystallization of TS-1 zeolite, which include inducing $Ti(OH_2)_2(OH)_2(OSi)_2$ formation, promoting Ti and Si to form TS-1 framework at a matched rate, and facilitating to form micro-mesoporous TS-1 crystals by particle attaching. The obtained TS-1 catalysts assisted by AM exhibit excellent activity, recoverability and stability in various ODS reactions involving bulky sulphur-containing organic compounds, which also affirms the higher activity of Ti $(OH_2)_2(OH)_2(OSi)_2$ than the conventional $TiO_4$ species. Furthermore, the in-depth underlying reasons for the exceptional catalytic activity of $Ti(OH_2)_2(OH)_2(OSi)_2$ species in ODS was elucidated for the first time by density functional theory (DFT) calculations.

## 2. Experimental section

### 2.1. Materials

Tetraethyl orthosilicate (TEOS; 98 %) and tetrabutyl orthotitanate (TBOT; 98 %): Sinopharm. Tetrapropylammonium hydroxide solution (TPAOH; 25 wt%), dibenzothiophene (DBT; 99 %), N,N′-dimethylethylenediamine (97 %), and 4,6-Dimethyldibenzothiophene (4,6-DMDBT; 98%): Innochem Science & Technology. Acrylamide, n-octane (97 %) and n-hexadecane: Tianjin Fuchen Chemical Reagent Factory. L-Glutamine (99 %) and Tert-butyl hydroperoxide solution (TBHP; 70 wt%): Alfa Aesar (China) Chemicals. Formamid (98 %): Tianjin Yongsheng fine chemical co., ltd. Urea (99 %): Beijing Chemical Works. Diethylenetriamine (99 %), thiophene (99 %): Aladdin. Thianaphthene (BT; 99 %): Energy chemical. All these materials were used without further purification.

### 2.2. Synthesis of catalysts

#### 2.2.1. Syntheses of X-TS-95 series samples

X-TS-95 samples were synthesized assisted with different amide/amine additives through a two-step hydrothermal route under static conditions from the starting gels with the molar compositions of $SiO_2$: 0.025 $TiO_2$: 0.28 TPAOH: 28 $H_2O$: 0.095 X, X represents different amide/amine additives. AM-TS-0 as the control sample was synthesized under the similar conditions without any additive. Typically, the TPAOH solution was mixed with water under stirring. Then, TBOT and TEOS were added to the TPAOH solution to form a clear solution under continuous stirring. After complete hydrolysis of TEOS and TBOT, the additives were added into the above solution. The reaction mixture was further stirred for hours until the solution becomes uniform. Finally, the resulting solution was transferred into a Teflon-lined stainless-steel autoclave and then crystallized in a pre-heated oven at 80 °C for 3 h, and then at 120 °C for 12 h under static conditions. The as-synthesized solid products were centrifuged, washed with distilled water several times, and dried at 80 °C in an oven overnight, then followed by calcination at 550 °C for 6 h.

#### 2.2.2. Syntheses of AM-TS-x series samples

TS-1 zeolites with different amount of AM were synthesized under the similar conditions as control sample of AM-TS-0. The molar compositions of synthesis gel are $SiO_2$: 0.025 $TiO_2$: 0.28 TPAOH: 28 $H_2O$: x

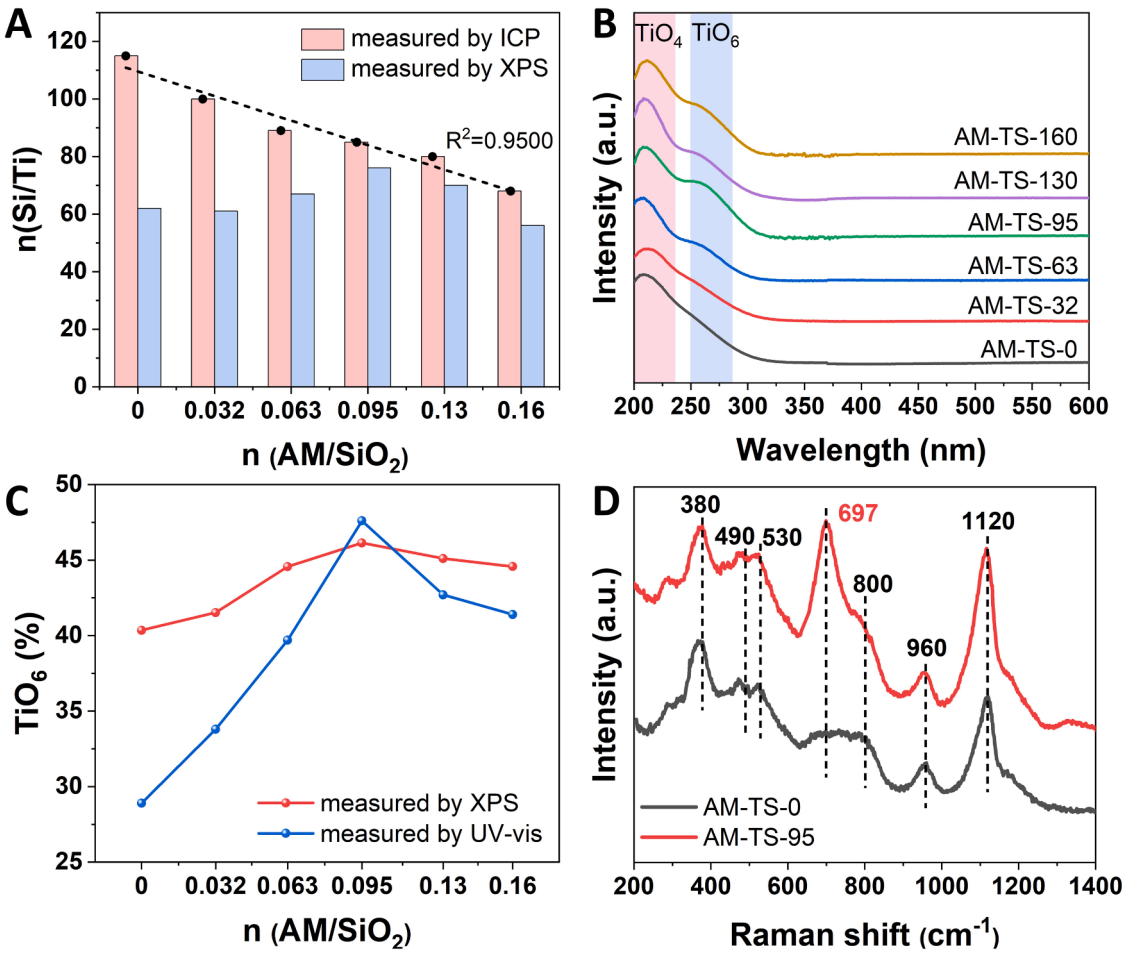


**Fig. 2.** (A) Si/Ti molar ratios determined by ICP and XPS, and (B) UV–vis spectra of samples synthesized with different AM amounts. (C) Percentage content of $TiO_6$ calculated from the peak areas by Gaussian fitting of XPS and UV–vis spectra of samples synthesized with different AM amounts. (D) UV-Raman spectra excited at 266 nm of AM-TS-0 and AM-TS-95.

AM, (x = 0, 0.032, 0.063, 0.095, 0.130, and 0.160). The obtained samples are named as AM-TS-x, where x represents the molar ratio of AM to $SiO_2$ times $10^3$ employed in the synthesis. The AM-TS-0 crystallized for 5 h is named AM-TS-0–5 h.

### 2.2.3. Acid treatment of AM-TS-95

1 g uncalcined AM-TS-95 sample was treated with 50 mL 3 M $HNO_3$ solution at 50 °C for 24 h, the obtained product was thoroughly washed with distilled water, then followed by calcination at 550 °C for 6 h, named as AM-TS-95-acid.

## 2.3. Catalytic reactions

A certain amount of DBT, 4,6-DMDBT, BT or Th was dissolved in n-octane respectively to prepare the model fuel with the concentration of sulfur is about 500 ppm. The ODS reactivity was tested in a 25 mL two-neck glass flask equipped with a reflux condenser. In a typical run, the reaction was carried out with 10 mL model fuel, 0.08 g of zeolite catalyst, 0.028 g of n-octadecane and 0.056 g of TBHP at 333 K for 30 min. Afterwards, GC-MS (Thermo Fisher Trace ISQ, equipped with a TG-5MS column, 60 m 320 μm 25 μm) was utilized to analyze the reactant and products. Furthermore, model oils with different sulfur concentrations were used to simulate various fuel oils in practice. The concentration of DBT, 4,6-DMDBT and BT was 300 ppm, 200 ppm and 100 ppm, respectively. Other reaction conditions were consistent with the above example.

The sulphide conversion was calculated by the following equation:

$$\alpha = \frac{C_0 - C_t}{C_0} \times 100\%$$

Where: α is the sulphide conversion (%); $C_0$ and $C_t$ stand for the initial concentration and the centration after $t$ minutes reaction of sulphide, respectively.

The turnover frequency (TOF) of the oxidation of sulphide was calculated as follow:

$$\mathrm{TOF} = \frac{n(sulphide)_{initial} \times \alpha}{n(Ti) \times Reaction \quad time}$$

Where: $n(sulphide)_{initial}$ is the initial mole of sulphide; and $n$(Ti) is the mole of Ti species in the catalyst.

The activation energy $E_a$, is calculated from the Arrhenius equation:

$$k = Ae^{-E_a/RT}$$

Where: $k$ is the observed rate constant; $A$ is the pre-exponential factor; $E_a$ is the activation energy (J $mol^{-1}$); $R$ is the universal gas constant (8.314 J $mol^{-1}K^{-1}$); and $T$ is the temperature (K).

## 3. Results and discussion

### 3.1. Amide/amine-assisted syntheses of TS-1 zeolites

To regulate the active-site coordination and microenvironment, a selection of small molecule amides and amines, varying in molecular

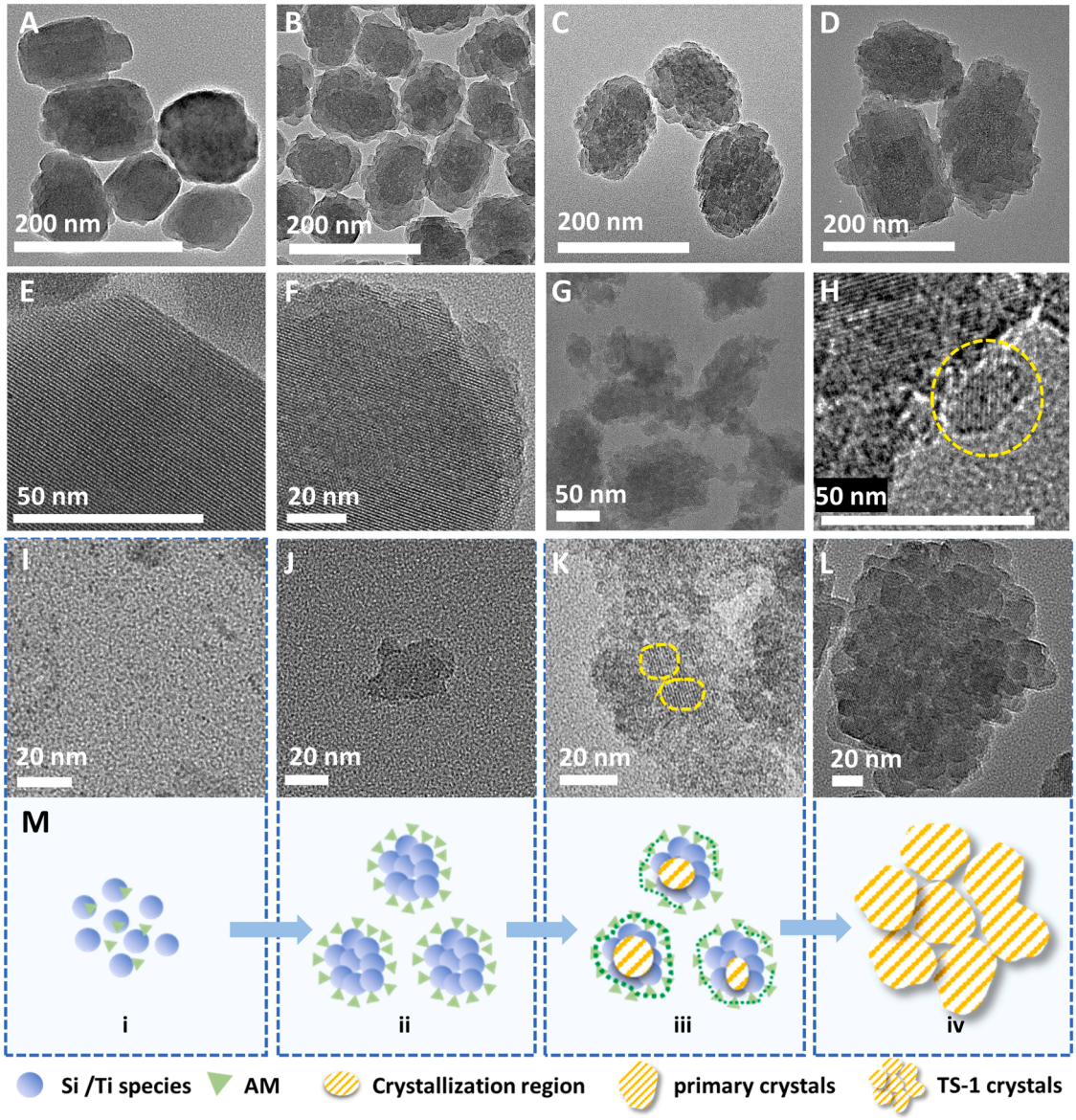


**Fig. 3.** TEM images of synthesized samples: (A) (E) AM-TS-0, (B) AM-TS-32, (C) (F)AM-TS-95, (D) AM-TS-160. AM-TS-95 crystallization for (I) 1 h, (J) 3 h, (K) 5 h, (G) (H) 7 h and (L) 10 h. (M) Scheme of the putative crystallization pathway of TS-1 in the presence of AM.

sizes and structures was employed as additives in the synthesis of TS-1 zeolite (Fig. 1 A). In the presence of these additives, all the synthesized samples exhibit typical **MFI** structural characteristics with good crystallinity (Fig. S1) and maintain nano-scaled sizes about 120–150 nm (Fig. S2). TG analysis proves that a small amount of additives are encapsulated in the samples (Fig. S3 and Table S1). Notably, the inclusion of these additives facilitates the incorporation of more Ti species into TS-1 crystals, resulting in lower n(Si/Ti) values than those of the control sample without any additive (Fig. 1B). By comparison, the amide-assisted samples contain a higher Ti content, display rougher surfaces and more obvious mesopores than amine-assisted samples (Fig. S2). The specific types of Ti sites in TS-1 samples are identified by UV–vis spectra. Typically, the peaks around 200–210 nm, 260 nm and 310 nm are attributed to tetra-coordinated $TiO_4$, hexa-coordinated $TiO_6$ ($Ti(OH_2)_2(OH)_2(OSi)_2$ or $Ti(OH)_4(OSi)_2$) and anatase $TiO_2$ species, respectively [28,35]. As depicted in Fig. S4 and Table S2, TS-1 without any additive (named as AM-TS-0) contains the highest proportion of $TiO_4$ (71.1 %) and the lowest proportion of $TiO_6$ (28.9 %). The introduction of additives could create more $TiO_6$ species in TS-1 zeolites, and the $TiO_6$ proportion follows the order of LG-TS-95 > AM-TS-95 > UREA-TS-95 > FA-TS-95 > DMAEA-TS-95 > -DETA-TS-95. It is noted that LG-TS-95 possesses the highest proportion of $TiO_6$ species (53.3 %), but with a small amount of anatase $TiO_2$ (4.6 %). In addition, anatase also exists in the presence of UREA, DMAEA and DETA. These results demonstrate that additives featuring diverse types and quantities of functional groups can effectively influence the amount and microenvironment of Ti species, and the introduction of AM is more conductive for the formation of $TO_6$ species in TS-1 zeolite.

The catalytic activity of the as-synthesized TS-1 samples was evaluated in the oxidative desulfurization reaction of dibenzothiophene (DBT). Obviously, the catalytic performance of TS-1 samples synthesized with amide or amine surpass that of the control sample as demonstrated by the time-course variation of DBT conversion (Fig. S5). The turnover frequency (TOF) follows the order of AM-TS-95 > LG-TS-95 > UREA-TS-95 > FA-TS-95 > DMAEA-TS-95 > DETA-TS-95, which appears to positively correlate with the proportion of $TiO_6$ species (Fig. 1 C). Among these samples, although LG-TS-95 contains the highest proportion of $TiO_6$, the presence of harmful $TiO_2$ makes its TOF lower compared to AM-TS-95. Consequently, AM-TS-95 containing more $TiO_6$ (47.6 %) without $TiO_2$ exhibits the highest TOF value

**Table 1**
Textural properties of synthesized TS-1 samples.

| | $S_{BET}$ ($m^2$ $g^{-1}$)[a] | $S_{micro}$ ($m_2$ $g^{-1}$)[b] | $S_{ext}$ ($m^2$ $g^{-1}$)[b] | $V_{total}$ ($cm^3$ $g^{-1}$)[c] | $V_{micro}$ ($cm^3$ $g^{-1}$)[d] | $V_{meso}$ ($cm^3$ $g^{-1}$)[e] |
|---|---|---|---|---|---|---|
| **AM-TS-0** | 480 | 351 | 129 | 0.46 | 0.15 | 0.31 |
| **AM-TS-32** | 500 | 368 | 132 | 0.48 | 0.15 | 0.33 |
| **AM-TS-63** | 530 | 313 | 217 | 0.48 | 0.13 | 0.35 |
| **AM-TS-95** | 531 | 312 | 219 | 0.51 | 0.13 | 0.38 |
| **AM-TS-130** | 536 | 306 | 230 | 0.52 | 0.12 | 0.40 |
| **AM-TS-160** | 539 | 343 | 196 | 0.59 | 0.14 | 0.45 |
| **AM-TS-95-acid** | 515 | 291 | 224 | 0.51 | 0.12 | 0.39 |
| **AM-TS-0–5 h** | 488 | 330 | 158 | 0.48 | 0.15 | 0.33 |

[a] Surface area was calculated from the nitrogen adsorption isotherm using the BET method.
[b] $S_{micro}$ (micropore area), $S_{ext}$ (external surface area) were calculated using the t-plot method.
[c] $V_{total}$ (total pore volume) at $P/P_0 = 0.99$.
[d] $V_{micro}$ (micropore volume) was calculated using the t-plot method.
[e] $V_{meso}$ (mesopore volume) = $V_{total}$ (total pore volume) - $V_{micro}$.

(134.8 $h^{-1}$), more than 3.0 times that of the control sample, and 1.6 times that of FA-TS-95 whose proportion of $TiO_6$ is lower (43.6 %).

### 3.2. Characterization of AM-assisted TS-1 catalysts

In view of the high activity of $TiO_6$ species in the oxidative desulfurization reaction of DBT, the prominent effect of AM on constructing $TiO_6$ species has been studied. A series of TS-1 zeolites were prepared by adjusting the amount of AM (n(AM/$SiO_2$): 0–0.16), and all of as-made samples possess well-defined **MFI** structures (Fig. S6). As depicted in Fig. 2 A, the overall Ti content of the samples gradually increase with the introduction of AM, a trend that is further corroborated by the results of $^{29}$Si MAS NMR analysis (Fig. S7) [37,38]. UV–vis spectra indicates that these samples all contain two kinds of active species, $TiO_4$ and $TiO_6$ (Fig. 2B). The proportion of $TiO_6$ species gradually increases with the addition of AM when n(AM/$SiO_2$) $\leq$ 0.095, while excessive AM leads to a reduction in $TiO_6$ content (Fig. 2 C, Fig. S8 and Table S3). Interestingly, the amount of AM also significantly impacts the distribution of Ti species. When n(AM/$SiO_2$) = 0.095, the relative content of $TiO_6$ on the surface is close to the overall $TiO_6$ relative content (46.2 % vs. 47.6 %), while for other cases, $TiO_6$ is primarily concentrated on the surface (Fig. 2 C and Fig. S9). Moreover, it was observed that the surface Si/Ti ratio of AM-TS-95 is closer to the overall ratio (76 vs. 85), suggesting a nearly uniform distribution of all types of Ti sites ($TiO_4$ and $TiO_6$) within the zeolite crystals (Table S3). High-angle annular dark-field scanning transmission electron microscopy (HAADF STEM) images and elemental mapping also confirm the homogeneous dispersion of Ti in the AM-TS-95 crystals (Fig. S10).

UV-Raman spectroscopy was conducted to identify the exact structure of $TiO_6$ species in the samples. As illustrated in Fig. 2D, the peaks at ~380 $cm^{-1}$ and ~800 $cm^{-1}$ are associated with the **MFI** topology, and the peak at ~960 $cm^{-1}$ is attributed to the vibration of the Si-O bond. The co-existence of the peaks at 490, 530 and 1120–1125 $cm^{-1}$ illustrate that there are tetra-coordinated framework $TiO_4$ species in both AM-TS-95 and AM-TS-0 in accordance with the UV–vis spectra results. Significantly, an obvious peak at 697 $cm^{-1}$ appears in AM-TS-95, which can be attributed to the $Ti(OH_2)_2(OH)_2(OSi)_2$ species [28,30,32,39]. As for AM-TS-0, a weak shoulder band at 697 $cm^{-1}$ is observed, possibly owing to its low $Ti(OH_2)_2(OH)_2(OSi)_2$ content [34,40]. It should be noted that other amide-assisted TS-1 zeolites also contain $Ti(OH_2)_2(OH)_2(OSi)_2$ species with characteristic peak is at 697 $cm^{-1}$, demonstrating the universal capability of amides for the construction of Ti $(OH_2)_2(OH)_2(OSi)_2$ species in TS-1 zeolite (Fig. S11).

More characterizations of AM-TS-x samples are performed to understand the fundamental role of AM in the crystallization of TS-1 zeolite. SEM images reveal that the average particle size of TS-1 increases from 89 nm to 136 nm with the increasing addition of AM (Fig. S12). This may be attributed to the stronger interconnections among AM molecules, resulting in a more heavily accumulation of primary crystals and, consequently, an enlargement of TS-1 crystal particle size [36]. TS-1 samples gradually exhibit aggregates formed through the accumulation of primary crystals (20–50 nm), generating numerous mesopores and making the crystal edges much rougher (Fig. 3A-F and Fig. S13). $N_2$ adsorption-desorption isotherms display a type I isotherm with hysteresis at the highest $P/P_0$ ratios (0.95–1.00), which signifies the presence of large interparticle mesopores in the samples (Fig. S14), and the Brunauer–Emmett–Teller (BET) surface area and mesoporous volume generally increase with the increase of AM (Table 1 and Fig. S15) [17,41]. These observations collectively suggest that AM significantly influences the formation process of TS-1 crystals.

By taking AM-TS-95 as an example, TEM images reveal the presence of small, dispersed Si/Ti oligomers after 1 h of crystallization (Fig. 3I). Subsequently, these oligomers form amorphous aggregates of ~ 20 nm after 3 h (Fig. 3J). After 5 h, these aggregates begin to partially crystallize, as denoted by the yellow circle in Fig. 3K.

Primary crystals with distinct lattice patterns are formed after 7 h (Figs. 3G, 3H and Fig. S16). Finally, TS-1 crystals are formed by particle attachment of these primary crystals (Fig. 3L) [42]. Combined with the results of dynamic light scattering (DLS), TG (Fig. S17 and Table S1) and $^{13}$C NMR (Figs. S18 and S19), it is rational to infer that AM is tightly bound to Si/Ti species through electrostatic interactions, hydrogen bonding or direct coordination, followed by partial polymerization at high temperatures as well as self-assembles by extensive hydrogen bonds, which may produce domain-limiting effects towards Si/Ti species during crystallization, resulting in the particle attachment for crystal growth to form TS-1 crystals with rough surfaces and rich mesopores (Fig. 3M). This role of AM is similar to the reported amino acid- and polymer-based additives in guiding hierarchical structures of zeolites [35,36].

### 3.3. Effects of AM on construction of $Ti(OH_2)_2(OH)_2(OSi)_2$ species

AM-TS-95 and AM-TS-0 are used as representatives to illustrate how AM affects exactly on active Ti sites by studying the process of Ti species incorporation into TS-1. As illustrated in Fig. S20, the introduction of AM could slow down the crystallization of TS-1. For AM-TS-95 sample, the relatively synchronous changes of Si and Ti species in the liquid component (Fig. 4 A) and in the solids (Fig. S21) indicate that Si and Ti species are transferred from the synthetic gel into solid phase at a comparable rate, resulting in homogeneous distribution of Ti species in the crystal [26]. Conversely, in the case of AM-TS-0 (Figs. S22 and S23), the rate of Si and Ti species entering TS-1 is inconsistent, and the Ti content showing a more pronounced increase during the 8–10 h crystallization, leading to rich Ti on the surface of the sample.

The evolution of Ti species in AM-TS-95 during its crystallization (6–12 h) was investigated using UV–vis spectroscopy. Ti species remain stable in the forms of $TiO_4$ and $Ti(OH_2)_2(OH)_2(OSi)_2$ from the initiation of crystallization (Fig. 4B). As crystallization progresses, there is a slight increase in the relative content of $TiO_4$, which is due to the continuous formation of **MFI** framework and the dehydration of part of Ti $(OH_2)_2(OH)_2(OSi)_2$ into $TiO_4$. In contrast, AM-TS-0 samples undergo crystallization between 5 and 10 h. In the early stages of crystallization, Ti species predominantly exist in the form of $TiO_4$. However, a small quantity of $Ti(OH_2)_2(OH)_2(OSi)_2$ emerges at 8 h and remains relatively constant until crystallization is complete (Fig. S24). This observation indicates that AM can induce the formation of $Ti(OH_2)_2(OH)_2(OSi)_2$ species in the early stage of crystallization and stabilize them throughout the entire process, rather than randomly generating them

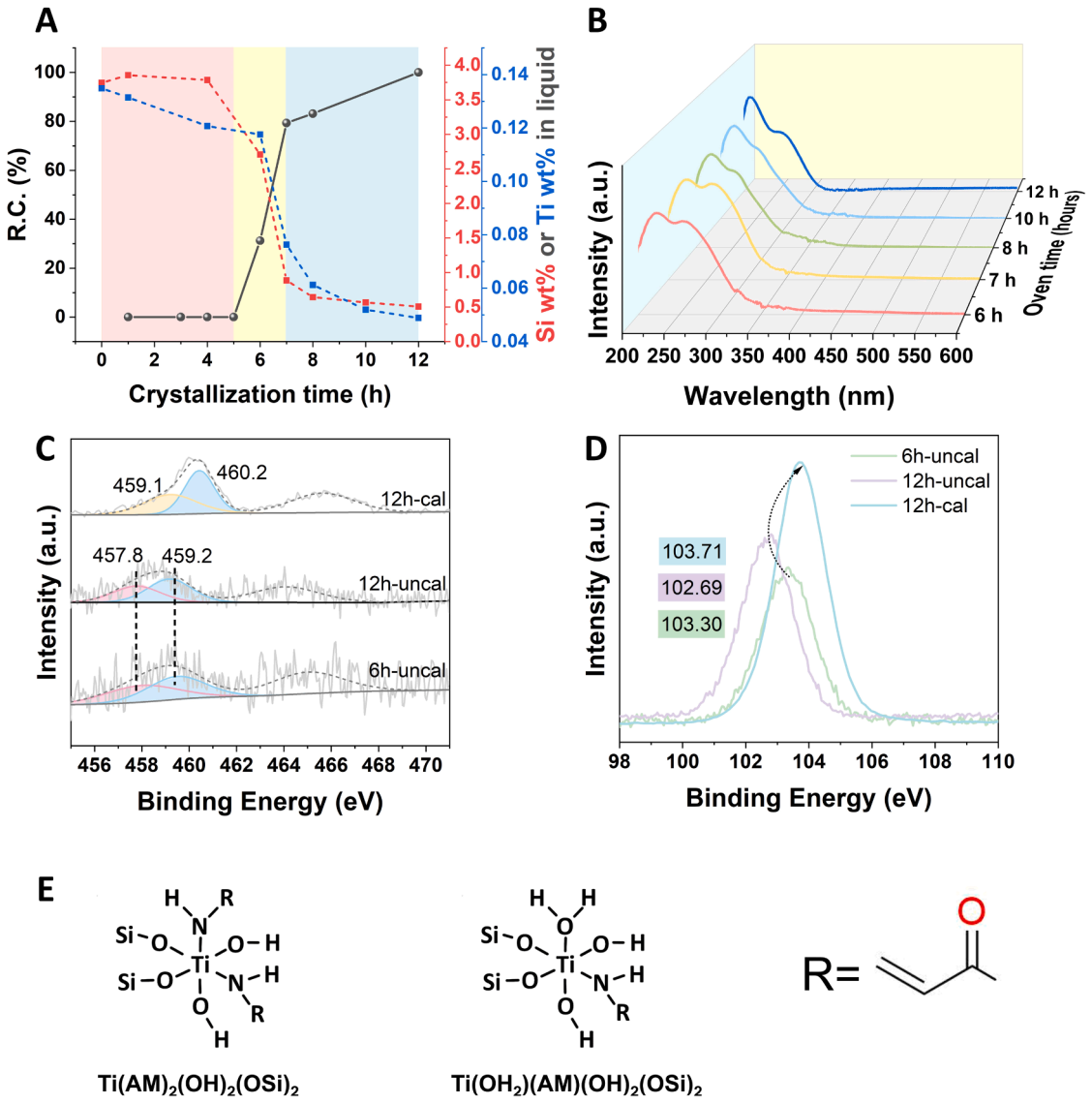


**Fig. 4.** (A) Evolution of the content of Si and Ti species in mother liquid supernatant of AM-TS-95. (B) UV–vis spectra of AM-TS-95 crystallized for different time. (C) XPS spectra of Ti 2p3/2 and (D) Si 2p in AM-TS-95–6 h-uncal, AM-TS-95–12 h-uncal and AM-TS-95 ("uncal" means uncalcined). (E) The proposed structure of Ti $(AM)_2(OH)_2(OSi)_2$ and $Ti(OH_2)(AM)(OH)_2(OSi)_2$ species.

later in the crystallization process.

XPS analysis is conducted to gain further insights into how AM induces the formation of $Ti(OH_2)_2(OH)_2(OSi)_2$, as depicted in Fig. 4 C. The peak at 457.8 eV is identified as a characteristic peak resulting from the strong interactions between the N atom of organic compounds and Ti species, leading to an increase in electrons density around Ti [43]. The N 1 s spectrum reveals the direct coordination between the $–NH_2$ groups of AM and Ti (Fig. S25) [44,45]. As illustrated in Fig. 4 C, AM is continuously coordinates with Ti throughout the entire crystallization in the forms of $Ti(AM)_2(OH)_2(OSi)_2$ and $Ti(OH_2)(AM)(OH)_2(OSi)_2$ species (Fig. 4E). After calcination, the organic ligands are replaced by $H_2O$ molecules, forming $Ti(OH_2)_2(OH)_2(OSi)_2$ species (the related peak at 457.8 eV moves to 459.1 eV), and subsequently, some of them are converted to $TiO_4$, resulting the increase in the content of $TiO_4$ [43]. As for the control sample AM-TS-0, only one peak appears at 459.2 eV at the early stage of crystallization (5 h), then a peak at 458.3 eV is observed as time progresses (Fig. S26), indicating that a small amount of $Ti(OH_2)_2(OH)_2(OSi)_2$ species is formed through coordination between the Ti species and -OH in solution during the late stages of crystallization. This type of construction may exhibit a severe randomness and uncertainty, as a result, resulting in the $Ti(OH_2)_2(OH)_2(OSi)_2$ species being mainly distributed on the surface of the sample. The interaction between AM and Si is also demonstrated by XPS spectra. As shown in Fig. 4D, the Si 2p peak in the uncalcined AM-TS-95 sample is obviously shifted towards low electronic energy compared to the calcined sample, and this shift is more pronounced than that observed in the peak of AM-TS-0 (Fig. S27), indicating a relatively strong interaction between Si and AM, so that Si and Ti can be "pulled" together by AM to form crystals [46,47].

Overall, the strong interaction of AM with both Si and Ti species in the early stages of crystallization allows AM to function as a bridging agent, slowing down crystallization while simultaneously facilitating the incorporation of Si and Ti species into TS-1 crystals at relatively equal rates, leading to the increase and homogeneous distribution of Ti species within the crystals. Particularly, the direct coordination between AM and Ti species in the gel leads to a large number of Ti species being stabilized in the form of $Ti(OH_2)_2(OH)_2(OSi)_2(AM)$, which subsequently enter the TS-1 crystals, and then transformed into $Ti(OH_2)_2(OH)_2(OSi)_2$ through the substitution of AM by $H_2O$.

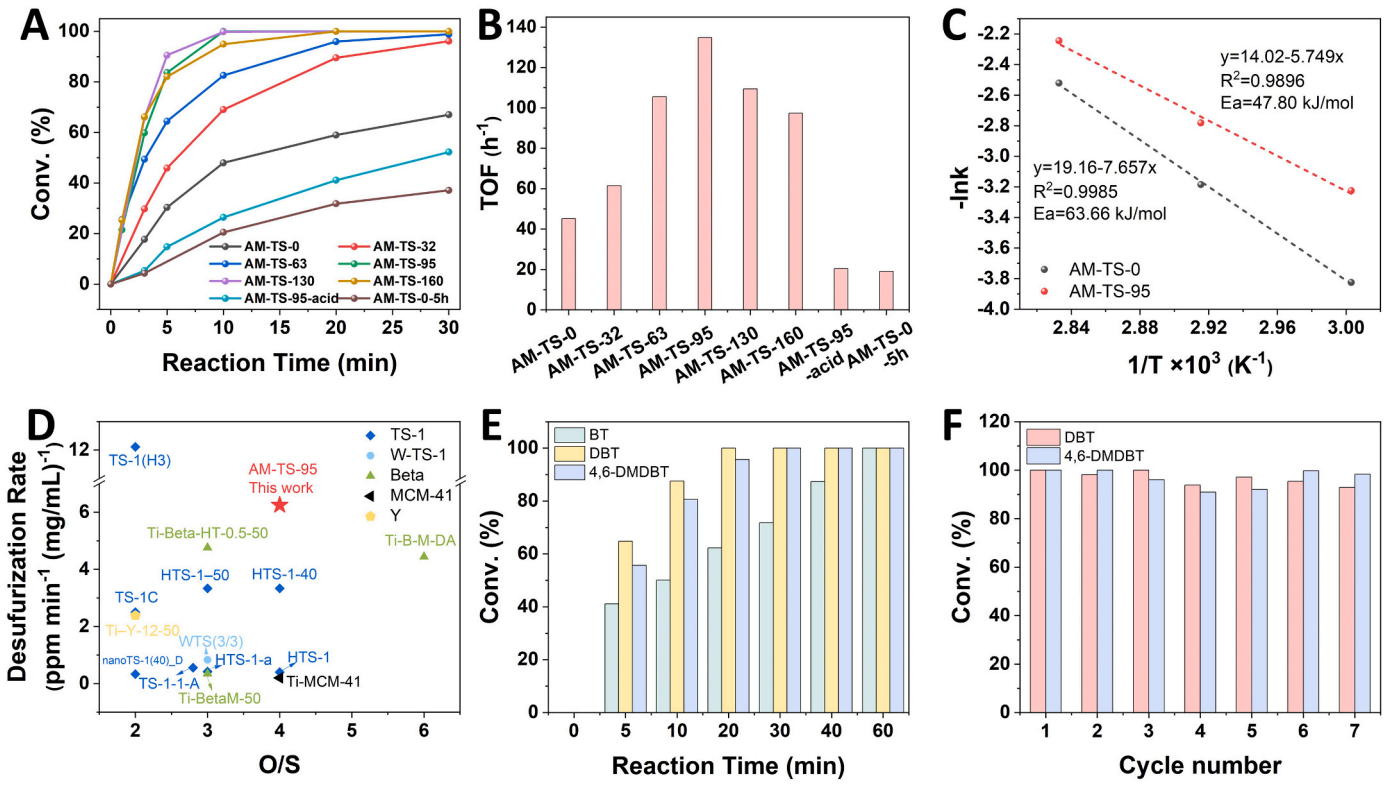


**Fig. 5.** (A) The conversion of DBT and (B) TOF of synthesized samples with different amount of AM. (C) Arrhenius plots for the conversion of DBT over AM-TS-0 and AM-TS-95. (D) Comparison of the catalytic activities of ODS of DBT over AM-TS-95 and the reports in literature. (E) Time-dependent conversion of simulated diesel oil including BT, DBT, and 4,6-DMDBT over AM-TS-95. (F) Reusability of AM-TS-95 in DBT and 4,6-DMDBT oxidation.

### *3.4. Evaluation of ODS performance*

Numerous studies have demonstrated the crucial role of the coordinated environment of Ti sites in TS-1 zeolite in catalytic applications [32,34]. In this study, the catalytic performance of AM-assisted TS-1 zeolites with rich $Ti(OH_2)_2(OH)_2(OSi)_2$ species are evaluated by the reaction of oxidative desulfurization using TBHP as the oxidant and n-octane as the solvent. The reaction scheme for the oxidative desulfurization of different sulfur-containing compounds to produce the corresponding sulfone ketone is shown in Fig. S28. The optimal reaction conditions were explored, indicating that the optimal conversion of DBT is achieved using 80 mg of catalyst and n(TBHP)/n(sulfur) (O/S) molar ratio of 4. It should be noted that an excessive amount of oxidant may reduce the accessibility of the active site by covering or blocking the pores, as depicted in Figs. S29-S31.

Fig. 5 A illustrates the catalytic performance of the synthesized TS-1 samples in typical DBT catalytic oxidation. Due to the small amount of Ti $(OH_2)_2(OH)_2(OSi)_2$ species, the control sample (AM-TS-0) exhibits slightly better activity than the general TS-1 catalyst, achieving a conversion of 48.0 % after 10 min and 67.0 % after 30 min [17]. TS-1 samples synthesized with AM have higher activity, in which AM-TS-95 and AM-TS-130 show significantly improved performance by achieving 100 % DBT conversion of DBT in just 10 min. Considering the different Ti content of these two samples, the reactivity of titanium sites is evaluated by calculating the TOF of Ti sites over each catalyst. As depicted in Fig. 5B, AM-TS-95 exhibits the highest TOF value (134.8 $h^{-1}$), which is 1.2 times that of AM-TS-130.

Notably, the TOF of these two samples is not directly correlated with the total Ti content but is closely related to the proportion of Ti $(OH_2)_2(OH)_2(OSi)_2$. When AM-TS-95 was washed with $HNO_3$ solution to remove almost all $Ti(OH_2)_2(OH)_2(OSi)_2$ but retaining the mesoporous structure (AM-TS-95-acid, Fig. S32), its conversion rate is greatly reduced, and only 26.4 % of DBT can be transformed within 10 min (for AM-TS-95 is 100 %). The TOF of Ti site also severely decreases from 134.8 $h^{-1}$ to 20.4 $h^{-1}$, revealing the higher activity of hexa-coordinated $Ti(OH_2)_2(OH)_2(OSi)_2$ than tetra-coordinated $TiO_4$ in DBT catalytic oxidation. In addition, to clarify the role of mesoporous structure in improving the catalyst activity, AM-TS-0–5 h, containing only $TiO_4$ species and lesser mesopore structure than that of AM-TS-95-acid (Fig. S33, Table 1) is chosen as a comparison. The TOF of AM-TS-0–5 h is 19.0 $h^{-1}$, similar with AM-TS-95-acid (20.4 $h^{-1}$). However, when extending the reaction time, the converted DBT over AM-TS-0–5 h is significantly less than that of AM-TS-95-acid. These results demonstrate that $Ti(OH_2)_2(OH)_2(OSi)_2$ species fundamentally determine the intrinsic activity of the catalyst and the mesoporous structure facilitates the contact of the substrate with the active site. Similar $Ti(OH_2)_2(OH)_2(OSi)_2$ species were discovered for the first time by Li and co-workers in TS-1 zeolites, which had been found to exhibit higher activity than $TiO_4$ in olefin epoxidation reactions [28,30]. However, its activity in ODS has not undergone in-depth studies.

Furthermore, AM-TS-95 and AM-TS-160 are selected for study the influence of $Ti(OH_2)_2(OH)_2(OSi)_2$ distribution on catalyst activity. Calculated based on n(Si/Ti) and percentages of $Ti(OH_2)_2(OH)_2(OSi)_2$ in the total Ti species of samples, the content of $Ti(OH_2)_2(OH)_2(OSi)_2$ in AM-TS-160 is 0.48 wt%, slightly higher than that in AM-TS-95 (0.45 wt %). However, AM-TS-95 shows higher conversion rate than AM-TS-160, over which the conversion is 100 % and 94.9 %, respectively, after 10 min (Fig. 5A). This may be attributed to the homogeneous distribution of $Ti(OH_2)_2(OH)_2(OSi)_2$ species (degree of distribution is 89.4 % vs. 82.3 % as shown in Table S3), which facilitates the accessibility of reactants to the active centers in AM-TS-95. In addition, the apparent activation energy ($E_a$) of AM-TS-95 is calculated to be 47.80 kJ $mol^{-1}$, much lower than that of AM-TS-0 (63.66 kJ $mol^{-1}$) (Fig. 5C, Fig. S34 and Fig. S35). This suggests that the oxidation of DBT has a lower reaction energy barrier and occurs more easily on AM-TS-95. Owing to the rich and homogeneously distributed $Ti(OH_2)_2(OH)_2(OSi)_2$ species, the

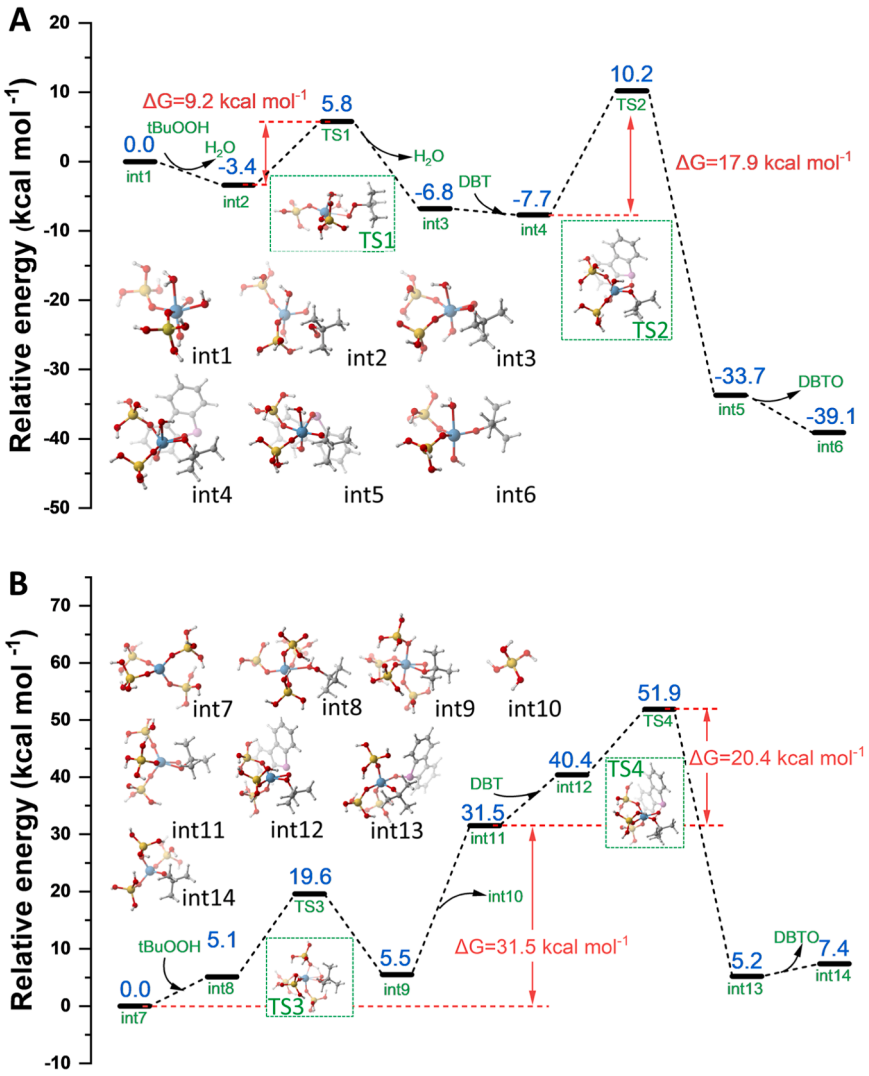


**Fig. 6.** Energy profiles for the oxidation reactions of DBT over (A) $Ti(OH_2)_2(OH)_2(OSi)_2$ site and (B) $TiO_4$ site.

desulfurization rate of AM-TS-95 catalyst is 6.25 ppm $min^{-1}$ (mg/mL)$^{-1}$, which is among the top level over other reported Ti-containing zeolite catalysts under similar conditions (Fig. 5D) [10–15,17–23].

The desulfurization activity was further evaluated for a typical larger volume molecule, 4,6-DMDBT, in comparison to DBT over the prepared catalysts (Fig. S36). Compared with the removal of DBT, the capacity of AM-TS-95 to remove 4,6-DMDBT is significantly superior to that of AM-TS-0. After 20 min of reaction, AM-TS-95 achieved a conversion rate of 100 %, while AM-TS-0 only achieved a conversion rate of 37.6 %, which suggests that mesopores play a crucial role in the catalysis of larger volume substrates in AM-TS-95. When selecting BT and Th as reactants that are difficult to be oxidized because of the low electron density of S atom, AM-TS-95 also shows higher catalytic activity than AM-TS-0 (TOF in BT oxidation: 33.3 $h^{-1}$ vs 21.1 $h^{-1}$, TOF in Th oxidation: 5.65 $h^{-1}$ vs 2.91 $h^{-1}$) (Figs. S37 and S38) [5,48]. Since BT and Th are relatively smaller molecules compared to DBT, the contribution of mesopores to the enhancement of catalytic efficiency is limited, emphasizing the role of $Ti(OH_2)_2(OH)_2(OSi)_2$ species in improving catalytic activity. Moreover, various types of model oils with different sulfur concentrations are used to simulate the fuel oils in practical applications. AM-TS-95 catalyst exhibits efficient removal of simulated diesel oil by completely desulfurizing 300 ppm DBT, 200 ppm 4,6-DMDBT, and 100 ppm BT within 20 min, 30 min, and 60 min, respectively (Fig. 5E).

As a crucial factor for practical application, the stability of AM-TS-95 in ODS reaction is investigated. This catalyst exhibits commendable cycling stability, maintaining a 92.9 % conversion of DBT and a 98.4 % conversion of 4,6-DMDBT even after seven cycles (Fig. 5F). Compared to the fresh AM-TS-95, FT-IR spectrum of the uncalcined catalyst after the first cycle in the ODS of DBT appears new peaks at 1285, 1168 and 570 $cm^{-1}$, which are attributed to the characteristic vibration of -$SO_2$- in $DBTO_2$, arising from the coordination of the silanol groups in the sample with $DBTO_2$ through hydrogen bonding (Fig. S39). Thus, the adsorption of $DBTO_2$ could lead to the deactivation of the catalyst by blocking the pores and covering the active sites [49]. These obstructing organic matters can be effectively removed through a simple high-temperature treatment while maintaining the framework structure and Ti species (Figs. S40-S42 and Table S3). Therefore, systematic analysis and experiments provide compelling evidence that the AM-TS-95 zeolite possesses high activity, excellent recovery performance, and stability towards ODS reactions, which is resulted by the effect of the higher Ti $(OH_2)_2(OH)_2(OSi)_2$ content, the homogeneous Ti distribution and rich mesoporous structure.

### 3.5. DFT calculations of reaction pathways over the active site

Density functional theory (DFT) calculations were conducted to gain deeper insights into the mechanism of ODS reaction over different active Ti-sites in TS-1 zeolite [50,51]. The distinct structures of Ti

$(OH_2)_2(OH)_2(OSi)_2$ and $TiO_4$ entail slightly different catalytic pathways for ODS of DBT as shown in Fig. 6, in which the optimized structural models for different sites and intermediates used in the calculations are presented in Fig. S43.

Overall, the oxidation of DBT on $Ti(OH_2)_2(OH)_2(OSi)_2$ site is exothermic with an exotherm of 39.1 kcal $mol^{-1}$, while it is an endothermic process with a heat absorption of 7.4 kcal $mol^{-1}$ on $TiO_4$ site indicating that DBT oxidation occurs more readily in $Ti(OH_2)_2(OH)_2(OSi)_2$ species than in $TiO_4$. Specifically, in the case of $Ti(OH_2)_2(OH)_2(OSi)_2$ as the active center, $H_2O$ is removed from the Ti $(OH_2)_2(OH)_2(OSi)_2$ site under the reaction of TBHP, followed by intramolecular dehydration, resulting in the formation of a Ti-$\eta^2$-OO-tBu intermediate (int3). This process undergoes TS1, which involves crossing an activation energy barrier of 9.2 kcal $mol^{-1}$. Subsequently, intermediate int3 adsorbs DBT and O is transferred from the central Ti atom to the S atom of DBT to form the corresponding product complex (int5), which undergoes TS2 via the transition state and needs to cross an energy barrier of 17.9 kcal $mol^{-1}$. In contrast, this process undergoes TS3 on $TiO_4$ center, with the subsequent dissociation of Si-OH to form Ti-$\eta^2$-OO-tBu (int11), which requires crossing a very higher activation energy barrier of 31.5 kcal $mol^{-1}$. Afterwards, int11 adsorbs DBT and then the peroxide bond opens the ring to give the intermediate int13, which needs to overcome an energy barrier of 20.4 kcal $mol^{-1}$ through the transition state TS4, which is greater than the energy barrier that needs to be crossed on $Ti(OH_2)_2(OH)_2(OSi)_2$ [30,52–56].

Briefly, the oxidation of DBT on $Ti(OH_2)_2(OH)_2(OSi)_2$ sites requires a lower reaction energy barrier (17.9 kcal $mol^{-1}$) compared to $TiO_4$ (51.9 kcal $mol^{-1}$). This is supported by the easier formation of the reactive intermediate Ti-$\eta^2$-OO-tBu and enhanced adsorption DBT substrates on $Ti(OH_2)_2(OH)_2(OSi)_2$ sites, making it a much easier reaction pathway, thus leading to the higher catalytic activity of AM-TS-95 catalyst.

## 4. Conclusions

In summary, we developed a facile amide-assisted synthesis method for constructing rich and homogeneously distributed $Ti(OH_2)_2(OH)_2(OSi)_2$ species within hierarchical TS-1 zeolite. The multi-functional role of amide in the synthesis of TS-1 has been unveiled through comprehensive analyses. Firstly, it modulates the structure of Ti species and influences the active-site microenvironment by coordinating with the Ti monomer through the amine groups, resulting in the construction of $Ti(OH_2)_2(OH)_2(OSi)_2$ species. Secondly, the incorporation speed of Ti and Si into zeolite framework is balanced via strong interactions between Si/Ti species and AM, thus leading to a relative homogeneous distribution of Ti in the crystal. Thirdly, the self-polymerise of AM during the hydrothermal synthesis exerts a domain-limiting effect, enabling the creation of hierarchical crystals through particle attachment. The ODS of DBT, BT, Th and 4,6-DMDBT showcases the superior reactivity of $Ti(OH_2)_2(OH)_2(OSi)_2$ species over traditional $TiO_4$ species. The as-made TS-1 catalyst exhibits outstanding catalytic performance, achieving 100 % conversion of DBT and 4,6-DMDBT within 10 and 20 min, and maintaining removal rate of 92.9 % and 98.4 % after seven cycles, respectively. DFT calculations further validate that $Ti(OH_2)_2(OH)_2(OSi)_2$ species require lower energy barriers for the formation of reactive intermediates and the adsorption of DBT compared to $TiO_4$ species, thus promoting more facile DBT oxidation. The synthesis strategy presented in this work is expected to be further developed for precise control the active sites in titanium-containing zeolites, ultimately enhancing catalyst activity.

## CRediT authorship contribution statement

**Jiani Zhang:** Conceptualization, Formal analysis, Investigation, Writing – original draft. **Risheng Bai:** Formal analysis, Investigation. **Zhaochi Feng:** Formal analysis, Investigation. **Jiyang Li:** Conceptualization, Project administration, Supervision, Writing – review & editing, Funding acquisition.

## Declaration of Competing Interest

The authors declare no conflict of interest.

## Data availability

Data will be made available on request.

## Acknowledgements

This work was supported by the National Natural Science Foundation of China (Grant Nos. 22288101), the 111 Project (B17020) and the National Natural Science Foundation of China (Grant Nos. 22201094).

## Appendix A. Supporting information

Supplementary data associated with this article can be found in the online version at doi:10.1016/j.apcatb.2023.123339.

## References

[1] S. Guan, Z. Li, B. Xu, J. Wu, N. Wang, J. Zhang, J. Han, T. Guan, J. Wang, K. Li, Cyclodextrin-based deep eutectic solvents for efficient extractive and oxidative desulfurization under room temperature, Chem. Eng. J. 441 (2022), 136022, https://doi.org/10.1016/j.cej.2022.136022.
[2] G. Ye, H. Wang, W. Chen, H. Chu, J. Wei, D. Wang, J. Wang, Y. Li, In situ implanting of single tungsten sites into defective UiO-66(Zr) by solvent-free route for efficient oxidative desulfurization at room temperature, Angew. Chem. Int. Ed. 60 (2021) 20318–20324, https://doi.org/10.1002/anie.202107018.
[3] M. Craven, D. Xiao, C. Kunstmann-Olsen, E.F. Kozhevnikova, F. Blanc, A. Steiner, I. V. Kozhevnikov, Oxidative desulfurization of diesel fuel catalyzed by polyoxometalate immobilized on phosphazene-functionalized silica, Appl. Catal. B Environ. 231 (2018) 82–91, https://doi.org/10.1016/j.apcatb.2018.03.005.
[4] W. Jiang, X. An, J. Xiao, Z. Yang, J. Liu, H. Chen, H. Li, W. Zhu, H. Li, S. Dai, Enhanced oxygen activation achieved by robust single chromium atom-derived catalysts in aerobic oxidative desulfurization, ACS Catal. 12 (2022) 8623–8631, https://doi.org/10.1021/acscatal.2c01329.
[5] Z. Zhu, H. Ma, W. Liao, P. Tang, K. Yang, T. Su, W. Ren, H. Lu, Insight into tri-coordinated aluminum dependent catalytic properties of dealuminated Y zeolites in oxidative desulfurization, Appl. Catal. B Environ. 288 (2021), 120022, https://doi.org/10.1016/j.apcatb.2021.120022.
[6] K. Leng, Y. Sun, X. Zhang, M. Yu, W. Xu, Ti-modified hierarchical mordenite as highly active catalyst for oxidative desulfurization of dibenzothiophene, Fuel 174 (2016) 9–16, https://doi.org/10.1016/j.fuel.2016.01.070.
[7] G. Ye, Y. Gu, W. Zhou, W. Xu, Y. Sun, Synthesis of defect-rich titanium terephthalate with the assistance of acetic acid for room-temperature oxidative desulfurization of fuel oil, ACS Catal. 10 (2020) 2384–2394, https://doi.org/10.1021/acscatal.9b04937.
[8] G. Ye, Y. Sun, D. Zhang, W. Zhou, C. Lancelot, A. Rives, C. Lamonier, W. Xu, Hierarchical porous titanium terephthalate based material with highly active sites for deep oxidative desulfurization, Microporous Mesoporous Mater. 270 (2018) 241–247, https://doi.org/10.1016/j.micromeso.2018.05.025.
[9] X. An, W. Jiang, L. Zhu, L. Xu, J. She, J. He, W. Zhu, H. Li, Design of grain boundaries enriched nickel molybdate for enhanced catalytic oxidative desulfurization, Appl. Catal. B Environ. 333 (2023), 122779, https://doi.org/10.1016/j.apcatb.2023.122779.
[10] K. Leng, X. Li, G. Ye, Y. Du, Y. Sun, W. Xu, Ti-containing hierarchical Beta with highly active sites for deep desulfurization of fuels under mild conditions, Catal. Sci. Technol. 6 (2016) 7615–7622, https://doi.org/10.1039/c6cy01389a.
[11] G. Lv, S. Deng, Z. Yi, X. Zhang, F. Wang, H. Li, Y. Zhu, One-pot synthesis of framework W-doped TS-1 zeolite with robust Lewis acidity for effective oxidative desulfurization, Chem. Commun. 55 (2019) 4885–4888, https://doi.org/10.1039/c9cc00715f.
[12] H. Ma, H. Lin, X. Liu, H. Lu, Z. Zhu, In situ structural reconstruction triggers the hydrothermal synthesis of hierarchical Ti-Beta zeolites for oxidative desulfurization, Mater. Chem. Front. 5 (2021) 6101–6113, https://doi.org/10.1039/d1qm00704a.
[13] L. Li, W. Wang, J. Huang, R. Dun, R. Yu, Y. Liu, Z. Hua, Synthesis of hydrophobic nanosized hierarchical titanosilicate-1 zeolites by an alkali-etching protocol and their enhanced performance in catalytic oxidative desulphurization of fuels, Appl. Catal. A Gen. 630 (2022), 118466, https://doi.org/10.1016/j.apcata.2021.118466.
[14] H. Lin, J. Wang, B. Gao, K. Yang, G. Lv, S. Qi, Z. Zhu, H. Lue, Solvent-free and low template content synthesis of Ti-Beta zeolite via interzeolite transformation for oxidative desulfurization, Microporous Mesoporous Mater. 344 (2022), 112203, https://doi.org/10.1016/j.micromeso.2022.112203.

[15] H. Lin, J. Zhang, Q. Duan, K. Yang, W. Liao, S. Qi, H. Lu, Z. Zhu, Dealumination-controlled strategy mediates Ti-Y zeolite with cooperative active sites for selective oxidations, Catal. Sci. Technol. 12 (2022) 4837–4850, https://doi.org/10.1039/d2cy00808d.

[16] T.-K. Kim, S.-T. Yang, D.R. Park, I.K. Song, K.-E. Jung, W.-S. Ahn, Ti-MWW synthesis and catalytic applications in partial oxidation reactions, Top. Catal. 53 (2010) 470–478, https://doi.org/10.1007/s11244-010-9474-z.

[17] R. Bai, Q. Sun, Y. Song, N. Wang, T. Zhang, F. Wang, Y. Zou, Z. Feng, S. Miaob, J. Yu, Intermediate-crystallization promoted catalytic activity of titanosilicate zeolites, J. Mater. Chem. A 6 (2018) 8757–8762, https://doi.org/10.1039/c8ta01960f.

[18] Q. Du, Y.P. Guo, H. Duan, H. Li, Y.J. Chen, H.Z. Liu, Synthesis of hierarchical TS-1 zeolite via a novel three-step crystallization method and its excellent catalytic performance in oxidative desulfurization, Fuel 188 (2017) 232–238, https://doi.org/10.1016/j.fuel.2016.10.045.

[19] Q. Du, Y. Guo, P. Wu, H. Liu, Y. Chen, Facile synthesis of hierarchical TS-1 zeolite without using mesopore templates and its application in deep oxidative desulfurization, Microporous Mesoporous Mater. 275 (2019) 61–68, https://doi.org/10.1016/j.micromeso.2018.08.018.

[20] S. Du, Q. Sun, N. Wang, X. Chen, M. Jia, J. Yu, Synthesis of hierarchical TS-1 zeolites with abundant and uniform intracrystalline mesopores and their highly efficient catalytic performance for oxidation desulfurization, J. Mater. Chem. A 5 (2017) 7992–7998, https://doi.org/10.1039/c6ta10044a.

[21] Q. Lv, G. Li, H. Sun, Synthesis of hierarchical TS-1 with convenient separation and the application for the oxidative desulfurization of bulky and small reactants, Fuel 130 (2014) 70–75, https://doi.org/10.1016/j.fuel.2014.04.042.

[22] M. Shakeri, S.B. Dehghanpour, Rational synthesis of TS-1 zeolite to direct both particle size and framework Ti in favor of enhanced catalytic performance, Microporous Mesoporous Mater. 298 (2020), 110066, https://doi.org/10.1016/j.micromeso.2020.110066.

[23] H. Wang, G. Du, S. Chen, Z. Su, P. Sun, T. Chen, Steam-assisted strategy to fabricate anatase-free hierarchical titanium silicalite-1 single-crystal for oxidative desulfurization, J. Colloid Interface Sci. 617 (2022) 32–43, https://doi.org/10.1016/j.jcis.2022.02.121.

[24] D.P. Serrano, R. Sanz, P. Pizarro, I. Moreno, S. Medina, Hierarchical TS-1 zeolite as an efficient catalyst for oxidative desulphurization of hydrocarbon fractions, Appl. Catal. B Environ. 146 (2014) 35–42, https://doi.org/10.1016/j.apcatb.2013.05.025.

[25] X. Zhang, J. Que, Y. Hou, J. Lyu, Z. Liu, K. Lei, S. Yu, X. Li, L. Chen, B. Su, Hierarchical mesoporous-microporous TS-1 single crystal catalysts for epoxidation of allyl chloride, Chem. J. Chin. Univ. 42 (2021) 2529–2539. ⟨http://www.cjcu.jlu.edu.cn/CN/10.7503/cjcu20210134⟩.

[26] Z. Chen, L. Zhang, Y. Yu, D. Liu, N. Fang, Y. Lin, D. Xu, F. Li, Y. Liu, M. He, TS-1 zeolite with homogeneous distribution of Ti atoms in the framework: synthesis, crystallization mechanism and its catalytic performance, J. Catal. 404 (2021) 990–998, https://doi.org/10.1016/j.jcat.2021.11.001.

[27] W.O. Parker, R. Millini, Ti coordination in titanium silicalite-1, J. Am. Chem. Soc. 128 (2006) 1450–1451, https://doi.org/10.1021/ja0576785.

[28] Y. Wang, H. Yang, Y. Zuo, D. Tian, G. Hou, Y. Su, Z. Feng, X. Guo, C. Li, New penta- and hexa-coordinated titanium sites in titanium silicalite-1 catalyst for propylene epoxidation, Appl. Catal. B Environ. 325 (2023), 122396, https://doi.org/10.1016/j.apcatb.2023.122396.

[29] C.P. Gordon, H. Engler, A.S. Tragl, M. Plodinec, T. Lunkenbein, A. Berkessel, J. H. Teles, A.-N. Parvulescu, C. Coperet, Efficient epoxidation over dinuclear sites in titanium silicalite-1, Nature 586 (2020) 708–713, https://doi.org/10.1038/s41586-020-2826-3.

[30] Q. Guo, K. Sun, Z. Feng, G. Li, M. Guo, F. Fan, C. Li, A Thorough investigation of the active titanium species in TS-1 zeolite by in situ UV resonance Raman spectroscopy, Chem. Eur. J. 18 (2012) 13854–13860, https://doi.org/10.1002/chem.201201319.

[31] L. Wu, Z. Tang, Y. Yu, X. Yao, W. Liu, L. Li, B. Yan, Y. Liu, M. He, Facile synthesis of a high-performance titanosilicate catalyst with controllable defective $Ti(OSi)_3OH$ sites, Chem. Commun. 54 (2018) 6384–6387, https://doi.org/10.1039/c8cc02794c.

[32] L.Z. Wu, X.J. Deng, S.F. Zhao, H.M. Yin, Z.X. Zhuo, X.Q. Fang, Y.M. Liu, M.Y. He, Synthesis of a highly active oxidation catalyst with improved distribution of titanium coordination states, Chem. Commun. 52 (2016) 8679–8682, https://doi.org/10.1039/c6cc03318k.

[33] R. Bai, M.T. Navarro, Y. Song, T. Zhang, Y. Zou, Z. Feng, P. Zhang, A. Corma, J. Yu, Titanosilicate zeolite precursors for highly efficient oxidation reactions, Chem. Sci. 11 (2020) 12341–12349, https://doi.org/10.1039/d0sc04603e.

[34] W. Xu, T. Zhang, R. Bai, P. Zhang, J. Yu, A one-step rapid synthesis of TS-1 zeolites with highly catalytically active mononuclear $TiO_6$ species, J. Mater. Chem. A 8 (2020) 9677–9683, https://doi.org/10.1039/c9ta13851j.

[35] Y. Wang, L. Li, R. Bai, S. Gao, Z. Feng, Q. Zhang, J. Yu, Amino acid-assisted synthesis of TS-1 zeolites containing highly catalytically active $TiO_6$ species, Chin. J. Catal. 42 (2021) 2189–2196, https://doi.org/10.1016/S1872-2067(21)63882-2.

[36] J. Zhang, R. Bai, Y. Zhou, Z. Chen, P. Zhang, J. Li, J. Yu, Impact of a polymer modifier on directing the non-classical crystallization pathway of TS-1 zeolite: accelerating nucleation and enriching active sites, Chem. Sci. 13 (2022) 13006–13014, https://doi.org/10.1039/d2sc04544c.

[37] W. Fan, R.-G. Duan, T. Yokoi, P. Wu, Y. Kubota, T. Tatsumi, Synthesis, crystallization mechanism, and catalytic properties of titanium-rich TS-1 free of extraframework titanium species, J. Am. Chem. Soc. 130 (2008) 10150–10164, https://doi.org/10.1021/ja7100399.

[38] Y.-g Ren, J. Huang, Q. Lv, Y. Xie, A.-H. Lu, M. Haruta, Dual-component gas pretreatment for Au/TS-1: enhanced propylene epoxidation with oxygen and hydrogen, Appl. Catal. A Gen. 584 (2019), 117172, https://doi.org/10.1016/j.apcata.2019.117172.

[39] C. Li, G. Xiong, Q. Xin, J.K. Liu, P.L. Ying, Z.C. Feng, J. Li, W.B. Yang, Y.Z. Wang, G. R. Wang, X.Y. Liu, M. Lin, X.Q. Wang, E.Z. Min, UV resonance Raman spectroscopic identification of titanium atoms in the framework of TS-1 zeolite, Angew. Chem. Int. Ed. 38 (1999) 2220–2222, https://doi.org/10.1002/(sici)1521-3773(19990802)38:15<2220::aid-anie2220>3.0.co;2-g.

[40] X. Song, X. Yang, T. Zhang, H. Zhang, Q. Zhang, D. Hu, X. Chang, Y. Li, Z. Chen, M. Jia, P. Zhang, J. Yu, Controlling the morphology and titanium coordination states of TS-1 zeolites by crystal growth modifier, Inorg. Chem. 59 (2020) 13201–13210, https://doi.org/10.1021/acs.inorgchem.0c01518.

[41] L.-H. Chen, X.-Y. Li, G. Tian, Y. Li, J.C. Rooke, G.-S. Zhu, S.-L. Qiu, X.-Y. Yang, B.-L. Su, Highly stable and reusable multimodal zeolite TS-1 based catalysts with hierarchically interconnected three-level micro-meso-macroporous structure, Angew. Chem. Int. Ed. 50 (2011) 11156–11161, https://doi.org/10.1002/anie.201105678.

[42] Z.Z. Sheng, H. Li, K. Du, L. Gao, J. Ju, Y. Zhang, Y. Tang, Observing a zeolite nucleus (subcrystal) with a uniform framework structure and its oriented attachment without single-molecule addition, Angew. Chem. Int. Ed. 60 (2021) 13444–13451, https://doi.org/10.1002/anie.202102621.

[43] L. Xu, D.-D. Huang, C.-G. Li, X. Ji, S. Jin, Z. Feng, F. Xia, X. Li, F. Fan, C. Li, P. Wu, Construction of unique six-coordinated titanium species with an organic amine ligand in titanosilicate and their unprecedented high efficiency for alkene epoxidation, Chem. Commun. 51 (2015) 9010–9013, https://doi.org/10.1039/c5cc02321a.

[44] Y. Li, T. Gao, Y. Yao, Z. Liu, Y. Kuang, C. Chen, J. Song, S. Xu, E.M. Hitz, B. Liu, R. J. Jacob, M.R. Zachariah, G. Wang, L. Hu, In situ "chainmail catalyst" assembly in low-tortuosity, hierarchical carbon frameworks for efficient and stable hydrogen generation, Adv. Energy Mater. 8 (2018), 1801289, https://doi.org/10.1002/aenm.201801289.

[45] J. Yin, H. Xu, B. Wang, W. Tian, J. Yin, J. Jiang, P. Wu, Highly selective 1-pentene epoxidation over Ti-MWW with modified microenvironment of Ti active sites, Catal. Sci. Technol. 10 (2020) 6050–6064, https://doi.org/10.1039/d0cy00478b.

[46] S.P. Chenakin, G. Melaet, R. Szukiewicz, N. Kruse, XPS study of the surface chemical state of a $Pd/(SiO_2+TiO_2)$ catalyst after methane oxidation and $SO_2$ treatment, J. Catal. 312 (2014) 1–11, https://doi.org/10.1016/j.jcat.2014.01.008.

[47] X. Wang, K. Wang, C.A. Plackowski, A.V. Nguyen, Sulfuric acid dissolution of 4A and Na-Y synthetic zeolites and effects on Na-Y surface and particle properties, Appl. Surf. Sci. 367 (2016) 281–290, https://doi.org/10.1016/j.apsusc.2016.01.103.

[48] Z. Hasan, J. Jeon, S.H. Jhung, Oxidative desulfurization of benzothiophene and thiophene with $WOx/ZrO_2$ catalysts: Effect of calcination temperature of catalysts, J. Hazard. Mater. 205 (2012) 216–221, https://doi.org/10.1016/j.jhazmat.2011.12.059.

[49] L. Chen, J.-T. Ren, Z.-Y. Yuan, Increasing the utilization of SiBeta support to anchor dual active sites of transition metal and heteropolyacids for efficient oxidative desulfurization of fuel, Appl. Catal. B Environ. 305 (2022), 121044, https://doi.org/10.1016/j.apcatb.2021.121044.

[50] D.H. Wells, W.N. Delgass, K.T. Thomson, Evidence of defect-promoted reactivity for epoxidation of propylene in titanosilicate (TS-1) catalysts: a DFT study, J. Am. Chem. Soc. 126 (2004) 2956–2962, https://doi.org/10.1021/ja037741v.

[51] C.W. Yoon, K.F. Hirsekorn, M.L. Neidig, X. Yang, T.D. Tilley, Mechanism of the decomposition of aqueous hydrogen peroxide over heterogeneous TiSBA15 and TS-1 selective oxidation catalysts: insights from spectroscopic and density functional theory studies, ACS Catal. 1 (2011) 1665–1678, https://doi.org/10.1021/cs2003774.

[52] M. Li, Y. Wang, Y. Wu, M. Wang, D. Zhou, Structure and catalytic activity of a newly proposed titanium species in a Ti-YNU-1 zeolite: a density functional theory study, Catal. Sci. Technol. 7 (2017) 4105–4114, https://doi.org/10.1039/c7cy01470h.

[53] H. Wang, Y. Deng, R. Zhou, Aromatic sulfur compounds oxidation with $H_2O_2$ over fully coordinated and defect sites in Ti-beta zeolites: evaluation by density functional theory, Theor. Chem. Acc. 137 (2018), https://doi.org/10.1007/s00214-018-2241-0.

[54] H. Wang, M. Yu, Z. Lin, A DFT study on catalytic oxidative desulfurization with $H_2O_2$ over Ti-MWW zeolite, J. Mol. Model. 25 (2019), 106, https://doi.org/10.1007/s00894-019-3989-4.

[55] H. Bian, H. Zhang, D. Li, Z. Duan, H. Zhang, S. Zhang, B. Xu, Insight into the oxidative desulfurization mechanism of aromatic sulfur compounds over Ti-MWW zeolite: a computational study, Microporous Mesoporous Mater. 294 (2020), 109837, https://doi.org/10.1016/j.micromeso.2019.109837.

[56] H. Bian, F. Wang, S. Wu, H. Zhang, B. Xu, A DFT Study on the mechanism of catalytic oxidation desulfurization over Ti-MWW zeolite, J. Clust. Sci. 33 (2022) 2103–2112, https://doi.org/10.1007/s10876-021-02134-0.